

## Entanglement and quantum steering in a hybrid multipartite system


Amjad Sohail<sup>1,2,\*</sup>, Montasir Qasymeh<sup>2,†</sup> and Hichem Eleuch<sup>3,4</sup>

<sup>1</sup>*Department of Physics, Government College University, Allama Iqbal Road, Faisalabad 38000, Pakistan*

<sup>2</sup>*Electrical and Computer Engineering Department, Abu Dhabi University, Abu Dhabi 59911, United Arab Emirates*

<sup>3</sup>*Department of Applied Physics and Astronomy, College of Sciences, University of Sharjah, Sharjah 27272, United Arab Emirates*

<sup>4</sup>*Institute for Quantum Science and Engineering, Texas AM University, College Station, Texas 77843, USA*

 (Received 7 May 2023; revised 2 August 2023; accepted 16 November 2023; published 30 November 2023)

We consider a multipartite hybrid system that incorporates a microwave cavity, a yttrium-iron-garnet (YIG) magnetic sphere resonator, a mechanical resonator, and an  $LC$  electrical resonator. The entanglement and the quantum steering properties of this multipartite system are thoroughly investigated by considering practical parameters. The microwave cavity mode is directly coupled to the magnon, mechanical, and electrical modes via Kittel magnetostatics, radiation pressure, and adjustable capacitance of the  $LC$  configuration, respectively. We demonstrate tripartite entanglement among different modes, including indirectly coupled modes (such as magnon entanglement with mechanical and  $LC$  electrical modes) for operating temperatures up to 2 K. Furthermore, we observe the presence of asymmetric one-way steering, revealing that the mechanical oscillator and the  $LC$  resonant modes can steer the indirectly coupled magnon mode (yet in one direction while steering is not possible in the backward direction). The integration of the four interacting modes provides a variety of controlling degrees of freedom and makes the proposed multipartite system an attractive approach for a wide range of applications, including data processing and communication, sensing, and quantum technologies.

DOI: [10.1103/PhysRevApplied.20.054062](https://doi.org/10.1103/PhysRevApplied.20.054062)

### I. INTRODUCTION

Developments in quantum physics have progressed over the past several decades from the conceptual description of microscopic events to advanced practical applications [1]. Quantum information concepts have contributed to these advances [2] like quantum sensing [3,4], secure quantum communications [5,6], quantum entanglement, quantum teleportation [7–13] and foundations of quantum mechanics [14,15]. Current technological advances allow observing and testing the manipulation (and control) of quantum systems. These include photons, atoms and ions [16,17], mesoscopic superconducting and nanomechanical and optomechanical systems [18–21].

Recently, yttrium-iron-garnet (YIG) spheres (containing cavities with magnon modes) have emerged as one of the most popular candidates for the study of quantum phenomena [22–27]. Such a system exploits the Kittel mode, which is strongly coupled to microwave (MW) fields and offers a distinctive way of studying a strong coherent coupling regime, which is very arduous to address otherwise [28–31]. A system consisting of a YIG sphere and magnon

mode incorporated with a microwave cavity is reported by Li and co-workers in Ref. [32]. They showed phonon, magnon, and photon-mode entanglement in both bipartite and tripartite. The reported entanglement survives up to 200 mK. In Ref. [28,29], a double microwave cavity system with magnon coupling was considered and a strategy to illustrate asymmetric quantum steering, nonlocality, and enhanced entanglement between different biparties (that persists up to 250 mK) was demonstrated.

Optoelectromechanical devices operate in the gigahertz (GHz) regime. However, functioning such devices in the megahertz range would be very beneficial. A mechanically movable membrane that is capacitively coupled to a  $LC$  resonator was proposed to generate and manipulate quantum entanglement using optoelectromechanical devices in the megahertz regime [32–35]. Due to the low associated noise, such optoelectromechanical devices have wide applications ranging from signal detection in astronomy [36] to nuclear magnetic resonance imaging (NMRI) [37]. Over the past decade, there has been considerable progress in preparing quantum correlations in optoelectromechanical systems [38]. For example, Cai *et al.* presented an experimentally feasible scheme to entangle two microwave cavity modes via optomechanical modulation. Furthermore, Zhong *et al.* proposed a scheme for the

\*amjadsohail@gcuf.edu.pk

†montasir.qasymeh@adu.ac.ae

realization of entangling microwave and optical modes coupled electro-optomechanical system [39]. Similarly, Tesfy *et al.* investigated the entanglements' generation of an optoelectromechanical system and found that the optical, mechanical, and microwave modes can be simultaneously entangled to one another [40]. In a more recent study, Li and Groblacher presented a scheme for the existence of steady-state entanglement between a mechanical and an  $LC$  resonators [32]. They found that entanglement between a low-frequency  $LC$  resonator and a mechanical resonator can be generated by having a suitable microwave drive. In another interesting paper, Correa and collaborators proposed an efficient hybrid scheme for a capacitively coupled optoelectromechanical system with a two-level atomic ensemble [41]. They found that not only maximum entanglement can be achieved between the two-level atomic ensemble and the mechanical oscillator, but also the entanglement presents a certain robustness against the thermal bath. Furthermore, Zhou and collaborators have proposed an electric circuit model for microwave optomechanics [42]. Their scheme is based on an  $RLC$  parallel circuit that model the mechanical oscillator as a movable capacitor. In this way, they are able to propose a generic microwave electromechanical model analog to the standard optomechanical system.

In the present study, we propose a scheme to generate bi(tripartite) entanglements and quantum steering in a hybrid system that combines microwave cavity, YIG spheres, mechanical resonator, and  $LC$  resonator that are all correlated (directly or indirectly) by radiation pressure, magnetostrictive interaction, and adjustable capacitance. The main motivation of the present study is to provide an additional degree of freedom by incorporating a magnon mode that enjoys low thermal noise and high-frequency operation to reduce the impact of thermal fluctuations and improve performance. Also, such a modality enables strong coupling and information transfer between different physical systems with high fidelity. Owing to the fact that a bias voltage can induce strong coupling between a resonant  $LC$  circuit and a mechanical resonator, we consider the frequency of the  $LC$  resonator in the radio frequency domain and close to the mechanical resonator frequency [43,44]. These considered configurations offer interesting features because the conversion of radiofrequency-microwave (rf-MW) signals to microwave signals can be utilized to detect weak rf-MW signals with high sensitivity [44]. In addition, such systems could reduce the noise sources for low-frequency signals. These possible applications could be, for example, in medical imaging, navigation, radio astronomy, and quantum communications. Needless to say, it is possible to seize the benefit of particular features of each subsystem in such a quadripartite setup. Our results demonstrate the entanglement of the four different bipartitions. We also observe the one-way quantum steering between bipartitions. In addition, we also

presented tripartite entanglement by employing minimum residual cotangle. It is worth mentioning that entanglement in the present case shows enhanced robustness against environmental temperature.

The paper is organized as follows. In Sec. II, the Hamiltonian of the system is presented. In Sec. III, we derive the dynamical equations of the system by employing the standard quantum Langevin approach. The entanglement measurement of the described system is illustrated in Sec. IV. Numerical simulations and results are discussed in Sec. V. The significance of the proposed model is elaborated in Sec. VI. Finally, we present the concluding remarks in Sec. VII.

## II. HAMILTONIAN OF THE SYSTEM

The proposed system comprises a microwave cavity coupled with a mechanical oscillator, an  $LC$  circuit, and a YIG sphere as depicted in Fig. 1. An experimental realization of an appropriate mechanical oscillator could be a metal-coated nanomembrane, which is simultaneously coupled to a cavity via radiation pressure force and capacitively coupled to an  $LC$  resonator [43,44]. The capacitance of the  $LC$  circuit can easily be changed when the membrane oscillates under radiation pressure force. In addition, the magnons are considered to be quasiparticles, which can be understood as a collective excitation of a number of spins in a ferrimagnet. The frequency of the magnon is flexible and can be modulated via  $\omega_m = \gamma_0 \mathcal{B}$ , where  $\gamma_0$  is the gyromagnetic ratio and  $\mathcal{B}$  is the external magnetic field. In addition, we also assume the membrane frequency is much less than magnon frequency. This condition is necessary to form dispersive phonon-magnon interaction [45,46]. Such a quadripartite system is described by the following Hamiltonian ( $\hbar = 1$ ):

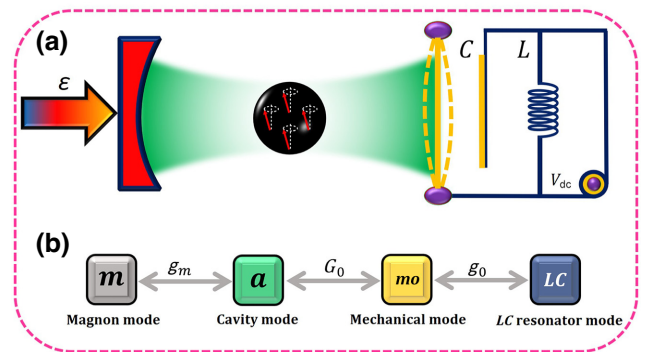


FIG. 1. (a) Schematic diagram of the proposed hybrid quadripartite system. The system consists of a microwave cavity that is simultaneously coupled to a magnon mode (via magnetostrictive interaction), a mechanical oscillator (via radiation pressure), and an  $LC$  circuit (via an adjustable capacitance). (b) The equivalent mode-coupling model.

$$H = H_o + H_I + H_d, \quad (1)$$

where

$$\begin{aligned} H_o &= \omega_a a^\dagger a + \omega_m m^\dagger m + \frac{\Omega_m}{2} (x^2 + p^2) + \frac{\omega_{LC}}{2} (q^2 + \phi^2), \\ H_I &= g_m (am^\dagger + a^\dagger m) - G_o a^\dagger ax + g_o x q^2, \\ H_d &= -\frac{q_o}{\hbar} q V + i\varepsilon (a^\dagger e^{-i(\omega_o t + \Phi)} - a e^{i(\omega_o t + \Phi)}), \end{aligned}$$

where  $a(a^\dagger)$  and  $m(m^\dagger)$  are the annihilation (creation) operator of the cavity mode with frequency  $\omega_a$  and the magnon mode with frequency  $\omega_m$ , respectively. Here,  $p$  and  $x$  are the momentum and position quadratures of the mechanical mode. Furthermore,  $\phi$  and  $q$  are the flux and charge quadratures of the  $LC$  resonator with frequency  $\omega_{lc} = 1/\sqrt{LC}$ . In the interaction Hamiltonian  $g_m$  represents the optomagnon coupling between the cavity and magnon mode. The one-photon optomechanical coupling is given by

$$G_o = \frac{\omega_a}{\mathcal{L}} \sqrt{\frac{\hbar}{m\Omega_m}}, \quad (2)$$

where  $\omega_a$  ( $\mathcal{L}$ ) is the frequency (length) of the cavity and  $\Omega_m$  ( $m$ ) is the frequency (mass) of the mechanical oscillator. The quantized  $LC$  circuit can be formed by an inductor  $L$ , a capacitor  $C$ , and a resistance  $R$ . The magnetic flux operator  $\phi$  and charge on capacitor  $q$  obey the standard commutation relation  $[q, \phi] = i$ . The membrane itself acts as a plate of the capacitor and therefore the capacitance of the capacitor depends on the mechanical resonator position. Hence, the electromechanical coupling is given by [41]

$$g_o = \frac{q_s q_o^2}{\hbar} \frac{dC^{-1}}{dx} \Big|_{x^s}, \quad (3)$$

where  $q_o = \sqrt{\hbar/L\omega_{LC}}$  ( $q_s$ ) represents the zero-point fluctuation (stationary mean charge) of the capacitor charge, and  $x^s$  is the membrane equilibrium position. Furthermore, the MW cavity is also driven by a field with phase  $\Phi$  and amplitude  $\varepsilon = \sqrt{\kappa_a \wp / \hbar \omega_0}$ , where  $\omega_0$  ( $\kappa_a$ ) is frequency (cavity leakage) while  $\wp$  denotes the power of external driving field.

The Hamiltonian of the system, in the rotating-wave approximation at the drive frequency  $\omega_0$ , can be written as

$$\begin{aligned} H &= \Delta_o a^\dagger a + \Delta_m m^\dagger m + \frac{\Omega_m}{2} (x^2 + p^2) + \frac{\omega_{LC}}{2} (q^2 + \phi^2) \\ &+ g_m (am^\dagger + a^\dagger m) - G_o a^\dagger ax + g_o x q^2 \\ &- \frac{q_o}{\hbar} q V + i\varepsilon (a^\dagger e^{-i\Phi} - a e^{i\Phi}), \end{aligned} \quad (4)$$

where  $\Delta_o = \omega_c - \omega_0$  and  $\Delta_m = \omega_m - \omega_0$ .

### III. QUANTUM DYNAMICS

The governing quantum Langevin equations (QLEs) of the considered system can be given by

$$\begin{aligned} \dot{a} &= -(i\Delta_o + \kappa_a) a - ig_m m + iG_o x a \\ &+ \varepsilon e^{-i\Phi} + \sqrt{2\kappa_a} a^{\text{in}}(t), \\ \dot{m} &= -(i\Delta_m + \kappa_m) m - ig_m a + \sqrt{2\kappa_m} m^{\text{in}}(t), \\ \dot{x} &= \Omega_m p, \\ \dot{p} &= -\Omega_m x - \gamma p + G_o a^\dagger a - g_o q^2 + \xi, \\ \dot{q} &= \omega_{LC} \phi, \\ \dot{\phi} &= \omega_{LC} q - \gamma_{LC} \phi - 2g_o x q + \frac{q_o}{\hbar} V. \end{aligned} \quad (5)$$

Here,  $\kappa_a$  ( $\kappa_m$ ) and  $\gamma$  ( $\gamma_{LC} = 2R/L$ ) are the decay rate of the cavity mode (magnon mode) and the damping rate of mechanical resonator ( $LC$  circuit). Furthermore,  $\xi$  and  $m^{\text{in}}$  ( $a^{\text{in}}$ ) are the vibrational mode and input noise operator for the magnon mode (cavity mode), respectively. The expectation value of these noise operators are zero. In addition, they obey the correlation relations [47] given by

$$\begin{aligned} \langle a^{\text{in}}(t) a^{\text{in}\dagger}(t') \rangle &= [n_a(\omega_a) + 1] \delta(t - t'), \\ \langle a^{\text{in}\dagger}(t) a^{\text{in}}(t') \rangle &= n_a(\omega_a) \delta(t - t'), \\ \langle m^{\text{in}}(t) m^{\text{in}\dagger}(t') \rangle &= [n_m(\omega_m) + 1] \delta(t - t'), \\ \langle m^{\text{in}\dagger}(t) m^{\text{in}}(t') \rangle &= n_m(\omega_m) \delta(t - t'). \end{aligned} \quad (6)$$

$n_j(\omega_j) = [e^{\hbar\omega_j/k_B T} - 1]^{-1}$  ( $j = a, m$ ), where  $k_B$  ( $T$ ) is the Boltzmann constant (temperature). Furthermore, the Brownian noise satisfies the relation:

$$\langle \xi(t) \xi(t') \rangle + \langle \xi(t') \xi(t) \rangle / 2 = \gamma_m [2n_m(\Omega_m) + 1] \delta(t - t').$$

To linearize QLEs, large  $LC$  circuit charge and cavity mode amplitude are considered, i.e.,  $q^s, |c\rangle \gg 1$ . Consequently, the QLEs can be linearized by writing  $o = o_s + \delta o$  ( $o_s = \langle o \rangle = a, m, x, p, q, \phi$ ), where  $o_s$  is the average value and  $\delta o$  is the fluctuation. It can be shown that the operators' average values are given by

$$\begin{aligned} a_s &= \frac{\varepsilon e^{-i\Phi} - ig_m m_s}{i\Delta_a + \kappa_a} = \frac{\varepsilon e^{-i\Phi}}{i\Delta_a + \kappa_a + \lambda}, \\ m_s &= \frac{-ig_m a_s}{i\Delta_m + \kappa_m}, \\ p_s &= \phi_s = 0, \\ x_s &= \frac{1}{\Omega_m} (G_o |a|^2 - g_o q_s^2), \\ q_s &= \frac{1}{\omega_{LC}} \left( \frac{q_o}{\hbar} V \right), \end{aligned} \quad (7)$$

where  $\Delta_a = \Delta_0 - G_0x$  is the modified normalized cavity detuning,  $\lambda = g_m^2/(i\Delta_m + \kappa_m)$ , and  $\omega_{LC} = \omega_L + 2g_0x_s$  is the resonance frequency of the LC circuit containing the frequency shift induced by the electromechanical interaction. In addition, the time dependency of the external bias voltage can be written as  $V(t) = V + \delta V(t)$ , where  $V$  is the dc bias voltage and  $\delta V(t)$  is the Johnson-Nyquist voltage fluctuation [48,49]. Here,  $\delta V(t)$  also represents the flux input noise and satisfies the Johnson-Nyquist noise correlation, reading

$$\langle \delta V(t)\delta V(t') \rangle = \left[ 4k_BTR + \gamma_{LC} \left( \frac{\hbar}{q_0} \right) \right] \delta(t-t'), \quad (8)$$

where  $R = \gamma_{LC}/(2)L$ . Consequently, if we use the Markovian approximation, for a large quality factor  $Q_{LC}$ , the above correlation function can be written as

$$\frac{1}{2} \langle \delta V(t')\delta V(t) + \delta V(t)\delta V(t') \rangle \simeq R\hbar\omega_{LC}[2n_{LC} + 1]\delta(t-t'), \quad (9)$$

where  $n_{LC} = [\exp(\hbar\omega_{LC}/k_B T) - 1]^{-1}$  represents the thermal excitation number in the LC circuit.

The steady-state field amplitude  $a_s$  is generally a complex quantity. However, in the real experimental scenario, we can have the choice to tune the driving field phase  $\Phi$ . Hence, we can consider  $a_s$  to be real and positive by taking a proper driving field phase  $\Phi$ . This assumption yields

$$a_s = \varepsilon \left[ (\kappa_a + |\lambda|^2 \kappa_m)^2 + (\Delta_a - |\lambda|^2 \Delta_m)^2 \right]^{-1/2}. \quad (10)$$

The real value of  $a_s$  indicates that the microwave photon in the cavity is coherently oscillating at a single frequency. Furthermore, this simplifies the analysis of the system because it means that the microwave photon and the mechanical oscillations are fully synchronized. To investigate the influence of the quantum fluctuations, considering a strong driving scenario, we can safely neglect the nonlinear cross-fluctuation terms (such as  $\delta a \delta x$  and  $\delta a^\dagger \delta a$ ) and obtain a linearized set for the QLEs (describing the evolution of the fluctuations operators), given by

$$\begin{aligned} \delta \dot{a} &= -(i\Delta_a + \kappa_a) \delta a - ig_m \delta m + iG_0 a_s \delta x + \sqrt{2\kappa_a} \delta a^{\text{in}}(t), \\ \delta \dot{m} &= -(i\Delta_m + \kappa_m) \delta m - ig_m \delta a + \sqrt{2\kappa_m} \delta m^{\text{in}}(t), \\ \delta \dot{x} &= \Omega_m \delta p, \\ \delta \dot{p} &= -\Omega_m \delta x - \gamma \delta p + G_0 a_s (\delta a + \delta a^\dagger) - 2g_0 q_s \delta q + \xi, \\ \delta \dot{q} &= \omega_{LC} \delta \phi, \\ \delta \dot{\phi} &= -\omega_{LC} \delta q - \gamma_{LC} \delta \phi - 2g_0 q_s \delta x + \frac{q_0}{\hbar} \delta V. \end{aligned} \quad (11)$$

The above set of QLEs can be used to describe the quadrature fluctuations  $(\delta X_a, \delta Y_a, \delta X_m, \delta Y_m, \delta x(t), \delta p(t), \delta q(t),$

$\delta \phi(t))$ , where  $\delta X_m = 1/\sqrt{2}(\delta m - \delta m^\dagger)$ ,  $\delta Y_m = 1/\sqrt{2}i(\delta m + \delta m^\dagger)$ ,  $\delta X_a = 1/\sqrt{2}(\delta a - \delta a^\dagger)$ ,  $\delta Y = 1/\sqrt{2}i(\delta a + \delta a^\dagger)$ . Consequently, the quadrature QLEs set can be given in a matrix form, as in the following:

$$\dot{\mathcal{C}}(t) = \mathcal{Z}\mathcal{C}(t) + \mathcal{N}(t), \quad (12)$$

where

$$\mathcal{Z} = \begin{pmatrix} \mathcal{Z}_{am} & \mathcal{Z}_G \\ \mathcal{Z}_G & \mathcal{Z}_{mLC} \end{pmatrix},$$

Each matrix is a  $4 \times 4$ , given by

$$\begin{aligned} \mathcal{Z}_{am} &= \begin{pmatrix} -\kappa_a & \Delta_a & 0 & g_m \\ -\Delta_a & -\kappa_a & -g_m & 0 \\ 0 & g_m & -\kappa_m & \Delta_m \\ -g_m & 0 & -\Delta_m & -\kappa_m \end{pmatrix}, \\ \mathcal{Z}_{mLC} &= \begin{pmatrix} 0 & \Omega_m & 0 & 0 \\ -\Omega_m & -\gamma & -G_q & 0 \\ 0 & 0 & 0 & \omega_{LC} \\ -G_q & 0 & -\omega_{LC} & -\gamma_{LC} \end{pmatrix}, \end{aligned}$$

and

$$\mathcal{Z}_G = \begin{pmatrix} 0 & 0 & 0 & 0 \\ G_a & 0 & 0 & 0 \\ 0 & 0 & 0 & 0 \\ 0 & 0 & 0 & 0 \end{pmatrix},$$

$$\begin{aligned} \mathcal{C}(t) &= [\delta X_a, \delta Y_a, \delta X_m, \delta Y_m, \delta x(t), \delta p(t), \delta q(t), \delta \phi(t)]^T, \\ \mathcal{N}(t) &= \left[ \sqrt{2\kappa_a} X_a^{\text{in}}(t), \sqrt{2\kappa_a} Y_a^{\text{in}}(t), \sqrt{2\kappa_m} X_m^{\text{in}}(t), \right. \\ &\quad \left. \sqrt{2\kappa_m} Y_m^{\text{in}}(t), 0, \xi(t), 0, \delta v \right]^T. \end{aligned}$$

Here,  $\delta v = q_0/(\hbar)\delta V$ , and  $\mathcal{C}(t)$  and  $\mathcal{N}(t)$  are the fluctuation and input noise vectors, respectively. The effective optomechanical and electromechanical coupling rates are given by  $G_a = \sqrt{2}G_0|a_s|$  and  $G_q = 2g_0q_s$ , respectively.

## IV. ENTANGLEMENT MEASUREMENT

### A. Bipartite entanglement

Our next step is to investigate the quantum correlation between various bipartitions at a steady state. The foremost task is to check the stability of the system, which occurs when the system reaches its steady state and shows entanglement only if the the eigenvalues (real parts) of the matrix  $\mathcal{Z}$  are negative [50]. Here, we achieved the stability conditions by employing the Routh-Hurwitz criterion [50]. The stability of the system is fully assured and will be discussed in the upcoming analysis. At steady state, the

covariance matrix (CM)  $\Gamma$  satisfies the Lyapunov equation [51,52], yielding

$$\mathcal{Z}\Gamma + \Gamma\mathcal{Z}^T = -\mathcal{D}, \quad (13)$$

where  $\mathcal{D} = \text{Diag}[\kappa_a, \kappa_a, \kappa_m, \kappa_m, 0, \gamma_m(2n_m + 1), 0, \gamma_{LC}(2n_{LC} + 1)]$ . The covariance matrix  $\Gamma$  can be represented as

$$\Gamma = \begin{pmatrix} \Lambda_a & \Theta_{a,m} & \Theta_{a,mo} & \Theta_{a,LC} \\ \Theta_{a,m}^T & \Lambda_m & \Theta_{m,mo} & \Theta_{m,LC} \\ \Theta_{a,mo}^T & \Theta_{m,mo}^T & \Lambda_{mo} & \Theta_{mo,LC} \\ \Theta_{a,LC}^T & \Theta_{m,LC}^T & \Theta_{mo,LC}^T & \Lambda_{LC} \end{pmatrix}. \quad (14)$$

Here,  $\Lambda_\beta(\beta)$  and  $\Theta_{\alpha,\beta}(\alpha, \beta)$  are  $2 \times 2$  matrices representing the local properties and the intermodel correlation of the cavity, magnon, mechanical and electrical modes, for  $\beta = a, m, mo, LC$ , respectively. Furthermore, each element of the covariance matrix can be extracted through the following expression:

$$\Gamma_{ij}(t) = \frac{1}{2} \langle \mathcal{C}_i(t')\mathcal{C}_j(t) + \mathcal{C}_j(t)\mathcal{C}_i(t') \rangle \quad (i, j = 1, 2, \dots, 8). \quad (15)$$

The bipartition degree of entanglement can be quantified by calculating the logarithmic negativity [51,53–56]:

$$E_N = \max[0, -\ln 2\eta^-], \quad (16)$$

where

$$\eta^- = 2^{-\frac{1}{2}} \left[ \sum [\varrho] - \sqrt{\sum [\varrho]^2 - 4 \det \varrho} \right]^{\frac{1}{2}}, \quad (17)$$

and

$$\sum [\varrho] = \det \varrho_a + \det \varrho_b - 2 \det \varrho_c. \quad (18)$$

Here,  $\varrho_n$  ( $n = a, b, c$ ) is  $2 \times 2$  block matrices. In addition,  $\sum [\varrho]$  and  $\det \varrho$  being the two symplectic invariants of the reduced covariance matrix for any two modes. Furthermore, the original covariance matrix  $\Gamma$ , which is of the order of  $8 \times 8$ , can be dimensioned to a submatrix  $\mathcal{V}_{in}$  of  $4 \times 4$  order of the two modes of interest, given by

$$\mathcal{V}_{in} = \begin{bmatrix} \mathcal{V}_{uu} & \mathcal{V}_{uv} \\ \mathcal{V}_{uv}^T & \mathcal{V}_{vv} \end{bmatrix}. \quad (19)$$

The diagonal entries of  $\mathcal{V}_{in}$  represent the reduced states of modes  $u$  and  $v$ .

## B. EPR steering

One distinct property of EPR steering of two interacting parties from entanglement is that EPR steering exhibits asymmetrical characteristics. The quantum steerability for two interacting modes in different directions can be expressed as [57,58]

$$\zeta_{\alpha|\beta} = \max\{0, \mathcal{S}(2\mathcal{V}_{uu}) - \mathcal{S}(2\mathcal{V}_{in})\}, \quad (20)$$

$$\zeta_{\beta|\alpha} = \max\{0, \mathcal{S}(2\mathcal{V}_{vv}) - \mathcal{S}(2\mathcal{V}_{in})\}. \quad (21)$$

Here,  $\mathcal{V}_{in}$  is given in Eq. (21), and the Rényi-2 entropy is given by

$$\mathcal{S}(v) = 2^{-1} \ln[\det(v)]. \quad (22)$$

In Eqs. (22) and (23),  $\zeta_{\alpha|\beta}$  (and  $\zeta_{\beta|\alpha}$ ) represents the steering in the direction from mode  $\alpha$  to mode  $\beta$  (and from mode  $\beta$  to mode  $\alpha$ ). Hence,  $\zeta_{\alpha|\beta} > 0$  ( $\zeta_{\beta|\alpha} > 0$ ) implies that the mode  $\alpha$  ( $\beta$ ) can steer the mode  $\beta$  ( $\alpha$ ) by Gaussian measurement. Now we outline some conditions for quantum steering between the  $\alpha$  and  $\beta$  modes: (i)  $\zeta_{\alpha|\beta} > 0$  and  $\zeta_{\beta|\alpha} > 0$  implies two-way steering, (ii)  $\zeta_{\alpha|\beta} > 0$  and  $\zeta_{\beta|\alpha} = 0$  (or  $\zeta_{\alpha|\beta} = 0$  and  $\zeta_{\beta|\alpha} > 0$ ) implies to one-way steering and finally (iii)  $\zeta_{\alpha|\beta} = \zeta_{\beta|\alpha} = 0$  corresponds to no-way steering.

## C. Tripartite entanglement

Tripartite entanglement among three parties is measured by the minimal residual contangle, defined as [56,59]

$$\mathcal{R}_\tau^{\min} \equiv \min[\mathcal{R}_\tau^{p|mb}, \mathcal{R}_\tau^{m|pb}, \mathcal{R}_\tau^{b|pm}], \quad (23)$$

where  $\mathcal{R}_\tau^{u|vx} \equiv C_{u|vx} - C_{u|v} - C_{u|x} \geq 0$  ( $x, u, v = a, m, b, \phi$ ) is the monogamy of quantum entanglement. This property ensures the invariance of the tripartite entanglement under all three permutations and hence represents a genuine three-way property among the three Gaussian modes [56,59,60]. Here,  $C_{l|m}$  can be well computed as the squared logarithmic negativity (i.e.,  $C_{l|m} = E_{l|m}^2$ ) representing the contangle of subsystems of  $l$  and  $m$ . For a tripartite scenario, we can compute the *one-mode-vs-two-modes* logarithmic negativity by redefining  $\eta^-$  [Eq. (16)] as

$$\eta^- = \min \text{eig} | \oplus_{j=1}^3 (-\sigma_y) \tilde{\mathcal{V}}_j |, \quad (24)$$

where  $\tilde{\mathcal{V}}_j = \mathcal{P}_{i|jk} \mathcal{V}_6 \mathcal{P}_{i|jk}$  ( $i \neq j \neq k$ ) with  $\mathcal{V}_6$  being the  $6 \times 6$  CM of the three modes of interest. Furthermore,  $\mathcal{P}_{1|23} = \sigma_z \oplus \mathbb{1} \oplus \mathbb{1}$ ,  $\mathcal{P}_{2|13} = \mathbb{1} \oplus \sigma_z \oplus \mathbb{1}$  and  $\mathcal{P}_{3|12} = \mathbb{1} \oplus \mathbb{1} \oplus \sigma_z$ , are partial transposition matrices at the level of the CM  $\mathcal{V}_6$ . Here,  $\sigma_y = [0, -i; i, 0]$  and  $\sigma_z = [1, 0; 0, -1]$ . Furthermore, the symbol  $\oplus$  expand the dimension of the matrices to  $(m+p) \times (n+q)$  of two matrices  $A$  with  $m \times n$  and  $B$  with  $p \times q$  dimension.

## V. RESULTS AND DISCUSSIONS

In this section, we discuss our numerical simulation findings for bipartite (tripartite) entanglement and quantum steering. The considered simulation parameters are consistent with the values reported in Refs. [43,44,46] (see Table I). These parameters are experimentally realizable making our system feasible with present-day technology. We consider four possible bipartitions, namely, (a)  $E_N^{m-m}$ , (b)  $E_N^{m-mo}$ , (c)  $E_N^{m-LC}$  and (d)  $E_N^{mo-LC}$  denoting the magnon-cavity, magnon-mechanical, magnon- $LC$ , and mechanical- $LC$  entanglements, respectively. Moreover, it is significant to indicate that  $E_N^{m-m}$  and  $E_N^{mo-LC}$  represent the directly coupled modes while  $E_N^{m-mo}$  and  $E_N^{m-LC}$  represent the indirectly coupled modes. In order to sufficiently cool the electrical mode and generate entanglement, the system requires strong coupling (i.e.,  $G_q > \kappa_a$ ). Hence, we consider the electromechanical coupling satisfying  $G_q \simeq 3\kappa_a$ . In addition, the frequency of the  $LC$  circuit can easily be tuned around the mechanical frequency of the membrane (i.e.,  $\omega_{LC} \approx \Omega_m$ ). Furthermore, the  $LC$  and the mechanical oscillators still show some thermal excitation because of their very low frequencies. Thus, the thermally excited mechanical mode should be cooled (de-excite) enough to generate entanglement in a quadpartite system. This can be achieved when a red-detuned external laser is used to drive the cavity, and thus, the mechanical mode is cooled adequately. The electrical mode in this way is also cooled thanks to the strong mechanical- $LC$  coupling. The  $LC$  and the mechanical oscillator modes cooling are essential to obtain the desired entanglement. We note that the optimal detunings  $-\Delta_m \simeq \Delta_a \simeq \Omega_m$  adopted here in the quadpartite system are analogs to those discussed in [12] to generate entanglement in a tripartite magnomechanical system.

The stability of the system can be addressed by the Routh-Herwitz criterion, imposing that the real part of all eigenvalues of the matrix  $\mathcal{Z}$  must be negative [50]. In other words, the stability condition restricts the system's

TABLE I. The simulation parameters used in our calculations (taken from recent reported experiments). All values are normalized with respect to  $\Omega_m$  frequency.

Parameters	Symbol	Value
Mechanical frequency	$\Omega_m$	$2\pi \times 10$ MHz
$LC$ circuit frequency	$\omega_{LC}$	$2\pi \times 10$ MHz
Cavity decay rates	$\kappa_a$	$2\pi \times 1$ MHz
Magnon decay rates	$\kappa_m$	$2\pi \times 0.5$ MHz
Mechanical damping rate	$\gamma_m$	$10^{-5}\Omega_m$
$LC$ circuit damping rate	$\gamma_{LC}$	$\simeq \gamma_m$
Magnon-cavity couplings	$g_m$	$2\pi \times 3.2$ MHz
Effective electromechanical coupling	$G_q$	$\simeq 3\kappa_a$
Temperature	T	15 mK
Mass of mechanical resonator	$m$	5 g

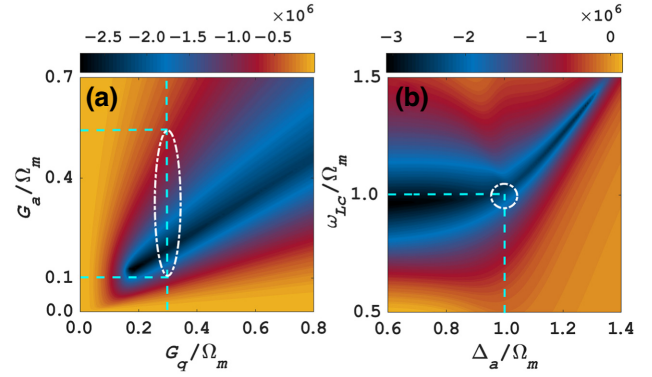


FIG. 2. The real part of the maximum eigenvalues of the drift matrix versus (a) the coupling rates  $G_q$  and  $G_a$  (b) the detunings  $\Delta_a/\Omega_m$  and  $\omega_{LC}/\Omega_m$ .

parameters to specific values where the system remains stable. Therefore, the foremost task is to check the regime for the parameters where stability occurs. In this regard, we initiate our numerical analysis first by verifying the eigenvalues of the matrix  $\mathcal{Z}$  (i.e.,  $|\mathcal{Z} - \lambda_{\mathcal{Z}}\mathbb{I}| = 0$ ) and ensuring satisfying the stability conditions. In Fig. 2(a) and 2(b), our numerical calculations show the contour plot of the maximum of the real part of the eigenvalues of the drift matrix  $\mathcal{Z}$  versus  $G_a/\Omega_m$  and  $G_q/\Omega_m$ , and  $\omega_{LC}/\Omega_m$  and  $\Delta_a/\Omega_m$ , respectively. We can see that the system is stable for specific parameter ranges. We use this map to select the parameter values that satisfy the stability conditions for all calculations throughout our numerical simulations presented in this work.

In Fig. 3(a), we present the four possible bipartitions versus  $\Delta_m$ , while  $\Delta_a = \Omega_m$ . It is shown that  $E_N^{m-mo}$  ceases to exist while the rest of the bipartition exhibits entanglement at  $\Delta_m = -\Omega_m$ . It is noteworthy that the two distant parties, i.e.,  $E_N^{m-LC}$ , show maximum entanglement exactly at  $\Delta_m = -\Omega_m$ . However,  $E_N^{m-mo}$  is ascendant, showing almost similar comportment as in Ref. [61]. It is also remarkable for a wide range of magnon detunings and has a maximum value for  $\Delta_m/\Omega_m = -0.65$ . On the other hand, the  $E_N^{mo-LC}$  is prominent for values of magnon detuning where  $E_N^{m-m}$ ,  $E_N^{m-mo}$  and  $E_N^{m-LC}$  are small. Indeed, the  $E_N^{mo-LC}$  is revoked in a short interval  $-0.75 \leq \Delta_m/\Omega_m \leq -0.45$  even at  $T = 10$  mK. Furthermore,  $E_N^{m-m}$ ,  $E_N^{m-mo}$ , and  $E_N^{m-LC}$  become almost equal when  $E_N^{mo-LC} = 0$  and  $\Delta_m = -0.75\Omega_m$ . Figures 3(b)–3(e) are the contour plots representing the four bipartitions for a range of cavity and magnon detunings, suggesting that we can achieve optimal entanglement of these bipartitions at different magnon and cavity detunings. We can easily conclude that the entanglement between different bipartitions can be (by design) redistributed through controlling the magnon and the cavity detunings.

Figure 4 displays the entanglement of the four bipartitions as a function of the effective coupling strengths

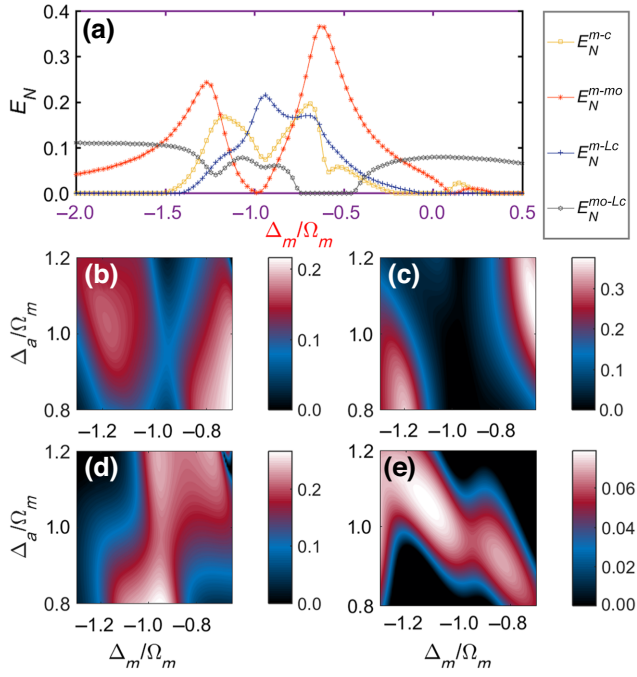


FIG. 3. (a) Entanglement of different bipartitions as a function of  $\Delta_m/\Omega_m$  for  $\Delta_a/\Omega_m = 1$ . Contour plot of bipartite entanglements (b)  $E_N^{m-m}$ , (c)  $E_N^{m-mo}$ , (d)  $E_N^{m-LC}$ , (e)  $E_N^{mo-LC}$  as a function of  $\Delta_m/\Omega_m$  and  $\Delta_a/\Omega_m$ . See Table I for other parameters.

$G_a$  and  $G_q$ . Here, the resonant case of  $\Delta_a = \omega_{LC} = \Omega_m$  is considered. The magnon detuning  $\Delta_m = -1.3\Omega_m$  is chosen as all four bipartitions show entanglement at this value. It is clear from Figs. 4(a) and 4(b) that the optimal value of  $E_N^{m-m}$  ( $E_N^{m-mo}$ ) takes place for values around

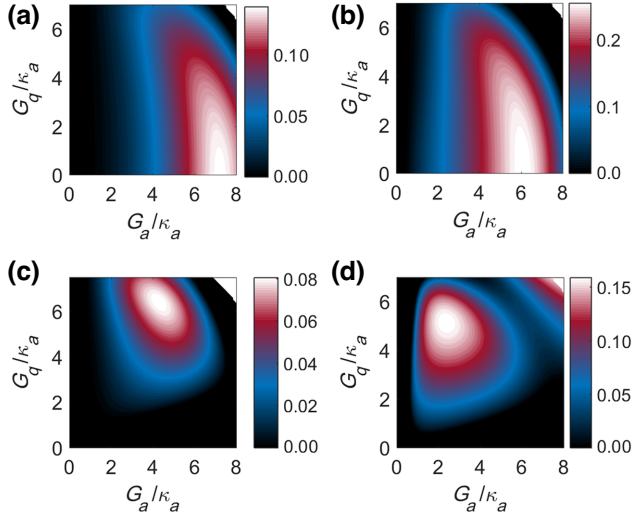


FIG. 4. Contour plot of bipartite entanglement as a function of the effective couplings  $G_a/\kappa_a$  and  $G_q/\kappa_a$ . (a)  $E_N^{m-m}$ , (b)  $E_N^{m-mo}$ , (c)  $E_N^{m-LC}$ , (d)  $E_N^{mo-LC}$ . Here, the resonance case  $\Delta_a = \omega_{LC} = \Omega_m$  is considered and  $\Delta_m = -1.3\Omega_m$ . See Table I for the parameters.

$G_a = 7\kappa_a$  ( $G_a = 6\kappa_a$ ) as well as for  $G_q \leq 3\kappa_a$ , indicating strong (weak) dependence of  $E_N^{m-m}$  and  $E_N^{m-mo}$  on  $G_a$  ( $G_q$ ). On the other hand, the optimal entanglements  $E_N^{m-LC}$  and  $E_N^{mo-LC}$  are limited to certain ranges of  $G_q$  and  $G_a$ , as can be inferred from Figs. 4(c) and 4(d). For entanglement  $E_N^{m-LC}$  ( $E_N^{mo-LC}$ ), it can be seen from Figs. 4(c) and 4(d) that the optimal values are achieved for  $3\kappa \leq G_a \leq 5\kappa$  and  $5\kappa \leq G_q \leq 7\kappa$  ( $2\kappa \leq G_a \leq 3\kappa$  and  $4\kappa \leq G_q \leq 6\kappa$ ). The effective coupling strengths and the degree of entanglement can be tuned by varying experimentally feasible parameters. For example, the effective optomechanical coupling  $G_a$  can be changed by controlling the external laser pump field amplitude  $\varepsilon$ , while  $G_q$  can be tuned by adjusting the applied dc bias voltage  $V_{dc}$ . Physically, the drive of LC circuit modifies the optomechanical nonlinearity and hence can alter the chaotic threshold and lifetime of a capacitively coupled electromechanical system. Therefore, the inclusion of the LC circuit allows additional control to avoid the noise sources between the control field and the signal. In this way, we infer that the present system provides an alternative avenue for the manipulation of entanglement and steering.

From Fig. 5(a), it can be seen that the optimal entanglement of  $E_N^{m-m}$  arises over a specific frequency range, that is  $0.7\Omega_m \leq \omega_{LC} \leq \Omega_m$  and  $0.8\Omega_m \geq \Delta_a \geq 1.2\Omega_m$ . Similarly, the  $E_N^{m-mo}$  optimal entanglement takes place when  $\Delta_a \geq 1.3\Omega_m$  and  $\omega_{LC} \leq 0.7\Omega_m$  as shown in Fig. 5(b). It is also clear that  $E_N^{m-mo}$  vanishes for  $\Delta_a = \Omega_m$ . Therefore, we can infer that the proper choice of  $\omega_{LC}$  and  $\Delta_a$  leads to the optimal entanglement of different bipartitions. Conversely, as can be seen from Figs. 5(c) and 5(d), the optimal entanglement  $E_N^{m-LC}$  ( $E_N^{mo-LC}$ ) is obtained for  $\Delta_a = \Omega_m$  and  $\omega_{LC} \simeq 0.8\Omega_m$  ( $\Delta_a = \omega_{LC} \simeq \Omega_m$ ), verifying that low effective temperatures and strong interactions between

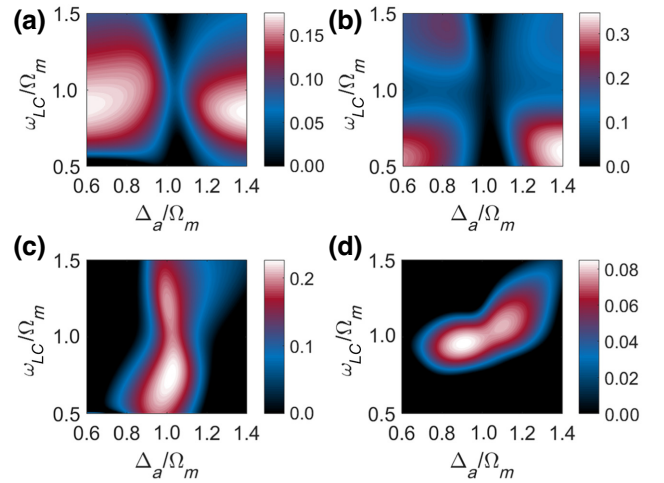


FIG. 5. Contour plot of bipartite entanglement (a)  $E_N^{m-m}$  (b)  $E_N^{m-mo}$  (c)  $E_N^{m-LC}$  (d)  $E_N^{mo-LC}$  as a function of  $\omega_{LC}/\Omega_m$  and  $\Delta_a/\Omega_m$ . Here,  $\Delta_m/\Omega_m = -1$ . See Table I for other parameters.

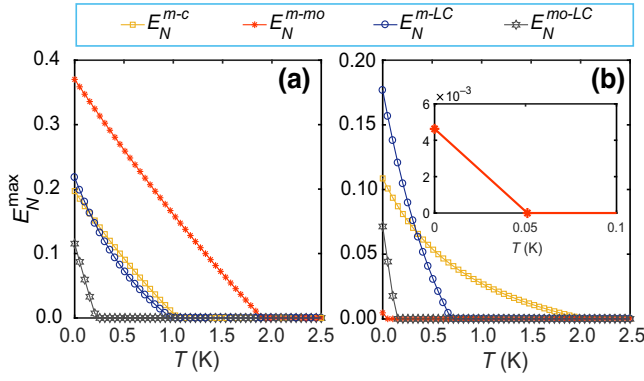


FIG. 6. The bipartite entanglements against temperature. (a) The optimal bipartite entanglements for an optimized  $\Delta_m$  detunings. (b) The bipartite entanglements under the condition of  $\Delta_m/\Omega_m = -1$ . See Table I for the parameters.

the electrical and the mechanical modes are a prerequisite for exhibiting their entanglement. We thus conclude that the present system offers an alternative platform to electrically control microwave signals through the entanglement process.

The robustness of the generated entanglements versus temperature is investigated in Fig. 6. In Fig. 6(a), the optimal entanglements of different bipartite subsystems (with optimized  $\Delta_m$  values) are presented. On the other hand, the entanglements are recalculated in Fig. 6(b) while considering  $\Delta_m = -\Omega_m$ . It can be seen that entanglements show contrasting behaviour for different tuning. For instance, while  $E_N^{m-LC}$  (blue circle line) ceases to exist around 1 K in Fig. 6(a), it rapidly drops off as temperature increases (surviving only up to 0.7 K) in Fig. 6(b). Conversely, while  $E_N^{m-m}$  (yellow square line) is being the second highest peak in Fig. 6(a) and preserving up to 1 K, it is more robust against environmental temperature in Fig. 6(b) and survives up to about 2 K (which is very much higher than the previous findings [12,28,29]). Lastly,  $E_N^{mo-LC}$  (gray star line) decreases monotonically in both cases while surviving only up to 250 and 200 mK in Figs. 6(a) and 6(b), respectively.

To investigate the impact of the magnon decay rate on the robustness of bipartite entanglements, we illustrate the optimal entanglements of various bipartition subsystems for different magnon detuning values in Figs. 7(a)–7(d). It can be seen that the two curves with larger magnon decay rates have a similar tendency, that is, the entanglement  $E_N^{m-m}$  and  $E_N^{m-mo}$  decrease with the increase of the temperature and there is a maximal entanglement at  $T = 0$ , which means that larger magnon decay rate possess stronger ability to resist decoherence of the thermal environment. In contrast,  $E_N^{m-m}$  decreases with the increase of the magnon decay rate. However,  $E_N^{mo-LC}$  remains unaffected by the rise of the magnon decay rate. Furthermore, it can also be shown from Fig. 7(e) that the entanglement  $E_N^{mo-LC}$

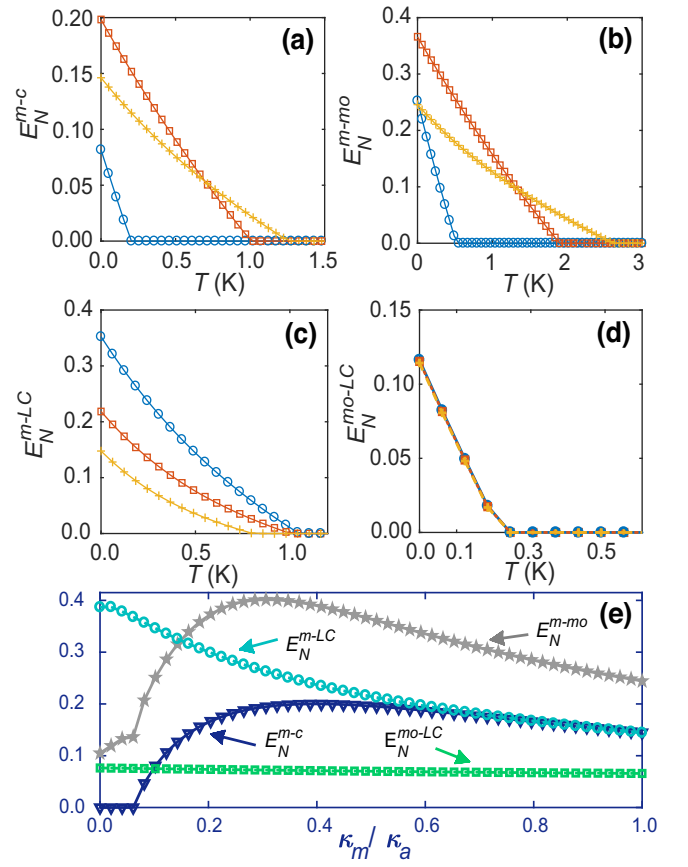


FIG. 7. (a),(d) Bipartite entanglements against temperature for the different choice of magnon detuning with  $\kappa_m = 0.1\kappa_a$  (blue-circle line),  $\kappa_m = 0.5\kappa_a$  (orange-square line) and  $\kappa_m = \kappa_a$  (yellow-plus line). (e) All bipartite entanglements against  $\kappa_m/\kappa_a$  for a fixed value of temperature. See Table I for the rest of the parameters.

can be transferred to  $E_N^{m-m}$  and  $E_N^{m-mo}$  for  $0 \leq \kappa_m/\kappa_a \leq 0.5$ . Thus, the magnon decay rate can also be used as an additional parameter to transfer and control entanglement in this quadpartite system.

In addition to our thorough analysis of bipartite entanglement for different subsystems, we also explore the asymmetric steering effect. In Figs. 8(a) and 8(b), we display the asymmetric one-way steering  $\zeta_{m|mo}$  and  $\zeta_{mo|m}$ . Furthermore, in Figs. 8(c) and 8(d), the asymmetric one-way steering  $\zeta_{m|LC}$  and  $\zeta_{LC|m}$  are presented considering  $\Delta_m = -\Omega_m$ . It is clear from Fig. 8, that the two indirect coupled modes (the mechanical and LC circuit modes) can steer the magnon mode. Yet, the magnon mode is not able to steer (backwardly) the mechanical and the LC circuit modes. The maximum steering  $\zeta_{mo|m}$  takes place when  $0.6 \geq \omega_{LC}/\Omega_m \geq 1.4$  and  $0.8 \geq \Delta_a/\Omega_m \geq 1.3$ , as shown in Fig. 8(b). However,  $\zeta_{m|mo} = 0$  for the reversed direction. Similarly, it can be clearly seen that the steering effect  $\zeta_{LC|m}$  takes place around  $\Delta_a/\Omega_m = 1$  for the  $\omega_{LC}/\Omega_m \in [0.5 \rightarrow 1.5]$  LC circuit frequency range. However, the



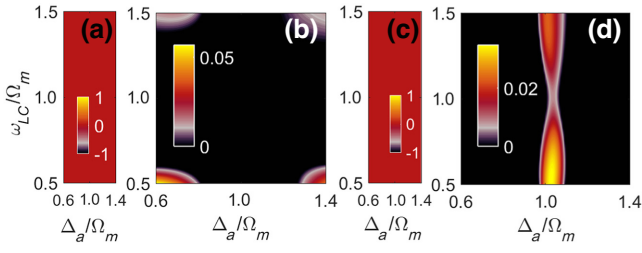


FIG. 8. The steerings (a)  $\zeta_{m|mo}$ , (b)  $\zeta_{mo|m}$ , (c)  $\zeta_{m|LC}$ , and (d)  $\zeta_{LC|m}$  densities versus  $\Delta_a/\Omega_m$  and  $\omega_{LC}/\Omega_m$ . In subplots (a) and (b),  $\Delta_m \simeq -0.4\Omega_m$ . In subplot (c) and (d),  $\Delta_m = -0.9\Omega_m$ . See Table I for the parameters.

maximum steering can be observed when  $\omega_{LC} < \Omega_m$  (i.e.,  $\omega_{LC} = 0.6\Omega_m$ ). These observations are explained by noting that steerable states are always entangled yet entangled states are not necessarily steerable [62]. In other words, to achieve Gaussian steering, a higher degree of quantum correlations between the two modes is necessary compared to what is required for entanglement. For instance, since the magnon mode is strongly correlated with the mechanical and the  $LC$  oscillators mode, steering effect is taking place. However, steering effect is not observed in other modes parties as they are weakly correlated. Furthermore, comparing Figs. 5(b) and 5(d) with Figs. 8(b) and 8(d), it is clear that the mechanical and the  $LC$  modes are entangled with the magnon mode; albeit they show steerability in one direction, which indicates the asymmetry nature of quantum correlations (one-way steering). In this regards, we note that the one-side device-independent quantum key distribution (QKD) is provided by one-way quantum steering, which has been experimentally realized [63,64].

Next, we study the tripartite entanglement among different parties. In Fig. 9(a), we show tripartite entanglement among the cavity, the magnon, and the mechanical modes, i.e.,  $\mathcal{R}_{m-c-mo}^{\min}$ . Figure 9(b) presents the tripartite entanglement among the cavity, the mechanical, and the  $LC$

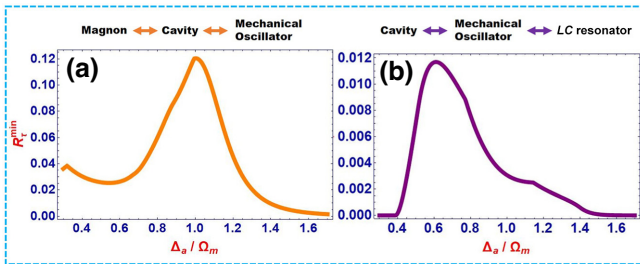


FIG. 9. Tripartite entanglements (in terms of the minimum residual contangle  $\mathcal{R}_t^{\min}$ ) versus  $\Delta_m/\Omega_m$ . The entanglement  $\mathcal{R}_{m-c-mo}^{\min}$  in (a) is among the cavity-magnon-mechanical modes when  $\Delta_m/\Omega_m = -0.7$ . The entanglement  $\mathcal{R}_{c-mo-LC}^{\min}$  in (b) is among the cavity-mechanical- $LC$  with  $\omega_{LC}/\Omega_m = 1$ . See Table I for the parameters.

modes, i.e.,  $\mathcal{R}_{c-mo-LC}^{\min}$ . It can be observed from Fig. 9(a) that the tripartite entanglement  $\mathcal{R}_{m-c-mo}^{\min}$  is maximized at  $\Delta_a = \Omega_m$ , which can be explained due to the strong bipartite entanglement between the magnon and the mechanical modes [as can be seen from Fig. 3(d)]. However, the  $\mathcal{R}_{c-mo-LC}^{\min}$  is almost 10 times smaller than  $\mathcal{R}_{m-c-mo}^{\min}$ . Furthermore, we observe the transfer of the tripartite entanglement from  $\mathcal{R}_{m-c-mo}^{\min}$  to  $\mathcal{R}_{c-mo-LC}^{\min}$  over the interval  $0.4 \leq \Delta_a/\Omega_m \leq 0.6$ , and from  $\mathcal{R}_{c-mo-LC}^{\min}$  to  $\mathcal{R}_{m-c-mo}^{\min}$  over the interval  $0.6 \leq \Delta_a/\Omega_m \leq 1$ .

## VI. SIGNIFICANCE OF THE PROPOSED MODEL

In this section, we aim to explore the advantages of integrating current hybrid systems into modern technological applications. Despite significant scientific advancements in operational speed and miniaturization, modern electronic equipment experiences inevitable rises in power consumption and Joule heating. Overcoming these constraints has sparked the search for alternative, charge-neutral information carriers. Consequently, a promising method for information encoding emerged: spin waves. As magnons (the quanta of spin waves) are not linked to the electron's translational motion, the risk of information loss is significantly reduced. Harnessing the phase and amplitude of magnons proves highly advantageous for signal transmission in magnon-assisted electro-optomechanical systems [65]. Recent studies have highlighted the potential of driving magnon-based devices using electric-field-induced methods to enhance efficiency, speed, and functionality in existing electronic devices [66,67]. Moreover, the low-frequency noise of magnons can aid in reducing quantum noise [68], thereby improving sensitivity, which is crucial for some applications such as gravitational-wave detection and producing EPR entangled sources [69].

In addition, the Coulomb modulation via adjustable capacitance in the present quadpartite system offers additional control capability. For instance, a recent experimental study by Calabrese *et al.* [70] demonstrated that Coulomb modulation becomes the dominant contribution to the total driving force for high-order mechanical modes. Such a system paves the way towards realizing coherent THz to optical transducers, enabling the development of fundamental optomechanical systems within the THz frequency range (0.1–10 THz). However, to date, the exploitation of Coulomb modulation in magnon-assisted electro-optomechanical systems is yet to be realized.

The amalgamation of low-loss information carriers, such as magnons, along with Coulomb modulation through electrical components and radiation pressure, is poised to forge another path in quantum information processing. Our obtained results in the present scheme not only pave the way for the next generation of devices but also offer enhanced control through Coulomb modulation. Consequently, we assert that our scheme has the potential

for applications in quantum information processing using readily available technology [1,71–73].

## VII. CONCLUSIONS

We have demonstrated an effective and straightforward approach to observe (bi)tripartite entanglement and quantum steering in a quadparty system that encompasses a microwave cavity that is simultaneously coupled to a magnon, a mechanical oscillator, and an  $LC$  oscillator mode. Each bipartition considered here has its own distinctiveness, which enriches the system dynamics and offers an extra degree of freedom. Our results reveal the necessary conditions to obtain entangled states for different associated subsystems. We have demonstrated that indirectly coupled modes exhibit optimal entanglement for properly chosen parameters. Moreover, we show that the entanglement of the indirectly coupled modes is still present for relatively high temperatures (up to 2 K). Furthermore, we have characterized the tripartite entanglement among different subsystems. One further noteworthy result demonstrates the existence of asymmetric one-way steering in which the mechanical and the  $LC$  resonators steer the magnon mode yet in one direction (i.e., the steering fails to exist in the opposite direction). We note here that a one-sided device-independent quantum key distribution is an example of a potential application that crucially needs the use of one-way steering.

All numerical data that support the findings in this study is available within the article.

## ACKNOWLEDGMENTS

This research is supported by ASPIRE, the technology program management pillar of Abu Dhabi's Advanced Technology Research Council (ATRC), via the ASPIRE Award for Research Excellence program.

- [1] G. Kurizki, P. Bertet, Y. Kubo, K. Mølmer, D. Petrosyan, P. Rabl, and J. Schmiedmayer, Quantum technologies with hybrid systems, *Proc. Natl. Acad. Sci.* **112**, 3866 (2015).
- [2] M. A. Nielsen and I. L. Chuang, *Quantum Computation and Quantum Information* (Cambridge University, Cambridge, UK, 2010).
- [3] C. Hempel, B. P. Lanyon, P. Jurcevic, R. Gerritsma, R. Blatt, and C. F. Roos, Entanglement-enhanced detection of single-photon scattering events, *Nat. Photonics* **7**, 630 (2013).
- [4] C. F. Ockeloen, R. Schmied, M. F. Riedel, and P. Treutlein, Quantum metrology with a scanning probe atom interferometer, *Phys. Rev. Lett.* **111**, 143001 (2013).
- [5] A. V. Sergienko, *Quantum Communications and Cryptography* (Taylor and Francis, Boca Raton, FL, 2006).
- [6] N. Gisin, G. Ribordy, W. Tittel, and H. Zbinden, Quantum cryptography, *Rev. Mod. Phys.* **74**, 145 (2002).
- [7] M. Qasymeh and H. Eleuch, Hybrid two-mode squeezing of microwave and optical fields using optically pumped graphene layers, *IEEE Photonics J.* **12**, 7500212 (2020).
- [8] M. Asjad, M. Qasymeh, and H. Eleuch, Continuous-variable quantum teleportation using a microwave-enabled plasmonic graphene waveguide, *Phys. Rev. Appl.* **16**, 034046 (2021).
- [9] A. Sohail, R. Ahmed, and C. S. Yu, Switchable and enhanced absorption via qubit-mechanical nonlinear interaction in a hybrid optomechanical system, *Int. J. Theor. Phys.* **60**, 739 (2021).
- [10] J. Li and S. Gröblacher, Entangling the vibrational modes of two massive ferromagnetic spheres using cavity magnomechanics, *Quantum Sci. Technol.* **6**, 024005 (2021).
- [11] R. Ahmed and S. Qamar, Optomechanical entanglement via non-degenerate parametric interactions, *Phys. Scr.* **92**, 105101 (2017).
- [12] J. Li, S. Y. Zhu, and G. S. Agarwal, Magnon-photon-phonon entanglement in cavity magnomechanics, *Phys. Rev. Lett.* **121**, 203601 (2018).
- [13] Y. C. Su and S. T. Wu, Entanglement enhancement through multirail noise reduction for continuous-variable measurement-based quantum-information processing, *Phys. Rev. A* **96**, 032327 (2017).
- [14] B. Hensen, H. Bernien, A. Reiserer, N. Kalb, and M. S. Blok, Loophole-free Bell inequality violation using electron spins separated by 1.3 kilometres, *Nature* **526**, 682 (2015).
- [15] L. K. Shalm *et al.*, Strong loophole-free test of local realism, *Phys. Rev. Lett.* **115**, 250402 (2015).
- [16] A. Aspuru-Guzik and P. Walther, Photonic quantum simulators, *Nat. Phys.* **8**, 285 (2012).
- [17] R. Blatt and C. F. Roos, Simulations with trapped ions, *Nat. Phys.* **8**, 277 (2012).
- [18] A. A. Houck, H. E. Türeci, and J. Koch, On-chip quantum simulation with superconducting circuits, *Nat. Phys.* **8**, 292 (2012).
- [19] R. J. Schoelkopf and S. M. Girvin, Wiring up quantum systems, *Nature* **451**, 664 (2008).
- [20] D. Vitali, S. Gigan, A. Ferreira, H. R. Böhm, P. Tombesi, A. Guerreiro, V. Vedral, A. Zeilinger, and M. Aspelmeyer, Optomechanical entanglement between a movable mirror and a cavity field, *Phys. Rev. Lett.* **98**, 030405 (2007).
- [21] L. Mazzola and M. Paternostro, Activating optomechanical entanglement, *Sci. Rep.* **1**, 199 (2011).
- [22] H. Huebl, C. W. Zollitsch, J. Lotze, F. Hocke, M. Greifenstein, A. Marx, R. Gross, and S. T. B. Goennenwein, High cooperativity in coupled microwave resonator ferromagnetic insulator hybrids, *Phys. Rev. Lett.* **111**, 127003 (2013).
- [23] Y. Tabuchi, S. Ishino, T. Ishikawa, R. Yamazaki, K. Usami, and Y. Nakamura, Hybridizing ferromagnetic magnons and microwave photons in the quantum limit, *Phys. Rev. Lett.* **113**, 083603 (2014).
- [24] X. Zhang, C. L. Zou, L. Jiang, and H. X. Tang, Strongly coupled magnons and cavity microwave photons, *Phys. Rev. Lett.* **113**, 156401 (2014).
- [25] A. Sohail, R. Ahmed, J. X. Peng, T. Munir, A. Shahzad, S. K. Singh, and Marcos César de Oliveira, Controllable

- Fano-type optical response and four-wave mixing via magnetoelastic coupling in an opto-magnomechanical system, *J. Appl. Phys.* **133**, 154401 (2023).
- [26] A. Sohail, R. Ahmed, C. S. Yu, and T. Munir, Tunable optical response of an optomechanical system with two mechanically driven resonators, *Phys. Scr.* **95**, 045105 (2020).
- [27] A. Sohail, R. Ahmed, J. X. Peng, A. Shahzad, and S. K. Singh, Enhanced entanglement via magnon squeezing in a two-cavity magnomechanical system, *J. Opt. Soc. Am. B* **40**, 1359 (2023).
- [28] A. Sohail, A. Hassan, R. Ahmed, and C. S. Yu, Generation of enhanced entanglement of directly and indirectly coupled modes in a two-cavity magnomechanical system, *Quantum Inf. Process.* **21**, 207 (2022).
- [29] A. Sohail, R. Ahmed, R. Zainab, and C. S. Yu, Enhanced entanglement and quantum steering of directly and indirectly coupled modes in a magnomechanical system, *Phys. Scr.* **97**, 075102 (2022).
- [30] S. Vashahri-Ghamsari, Q. Lin, B. He, and M. Xiao, Magnomechanical phonon laser beyond the steady state, *Phys. Rev. A* **104**, 033511 (2021).
- [31] B. Sarma, T. Busch, and J. Twamley, Cavity magnomechanical storage and retrieval of quantum states, *New J. Phys.* **23**, 043041 (2021).
- [32] J. Li and S. Gröblacher, Stationary quantum entanglement between a massive mechanical membrane and a low frequency LC circuit, *New J. Phys.* **22**, 063041 (2020).
- [33] E. A. Sete and H. Eleuch, Strong squeezing and robust entanglement in cavity electromechanics, *Phys. Rev. A* **89**, 013841 (2014).
- [34] R. W. Andrews, R. W. Peterson, T. P. Purdy, K. Cicak, R. W. Simmonds, C. A. Regal, and K. W. Lehnert, Bidirectional and efficient conversion between microwave and optical light, *Nat. Phys.* **10**, 321 (2014).
- [35] S. Barzanjeh, E. S. Redchenko, M. Peruzzo, M. Wulf, D. P. Lewis, G. Arnold, and J. M. Fink, Stationary entangled radiation from micromechanical motion, *Nature* **570**, 480 (2019).
- [36] M. J. Bantum, M. K. Verma, R. T. Rajan, A. J. Boonstra, C. J. M. Verhoeven, E. K. A. Gill, A. J. van der Veen, H. Falcke, M. Klein Wolt, B. Monna, S. Engelen, J. Rotteveel, and L. I. Gurvits, A roadmap towards a space-based radio telescope for ultra-low frequency radio astronomy, *Adv. Space Res.* **65**, 856 (2020).
- [37] M. Sarracanie, C. D. LaPierre, N. Salameh, D. E. J. Waddington, T. Witzel, and M. S. Rosen, Low-cost high-performance MRI, *Sci. Rep.* **5**, 15177 (2015).
- [38] Q. Cai, J. Liao, and Q. Zhou, Entangling two microwave modes via optomechanics, *Phys. Rev. A* **100**, 042330 (2019).
- [39] C. Zhong, X. Han, H. X. Tang, and L. Jiang, Entanglement of microwave-optical modes in a strongly coupled electro-optomechanical system, *Phys. Rev. A* **101**, 032345 (2020).
- [40] G. E. Tesfy and D. H. Alemu, Stationary entanglement dynamics in a hybrid opto-electro-mechanical system, *Rom. J. Phys.* **66**, 104 (2021).
- [41] C. Corrêa Jr. and A. Vidiella-Barranco, Quantum entanglement in a four-partite hybrid system containing three macroscopic subsystems, *Eur. Phys. J. Plus* **137**, 473 (2022).
- [42] X. Zhou, D. Cattiaux, D. Theron, and E. Collin, Electric circuit model of microwave optomechanics, *J. Appl. Phys.* **129**, 114502 (2021).
- [43] T. Bağcı, A. Simonsen, S. Schmid, L. G. Villanueva, E. Zeuthen, J. Appel, J. M. Taylor, A. Sørensen, K. Usami, A. Schliesser, and E. S. Polzik, Optical detection of radio waves through a nanomechanical transducer, *Nature* **507**, 81 (2014).
- [44] I. M. Haghghi, N. Malossi, R. Natali, G. Di Giuseppe, and D. Vitali, Sensitivity-bandwidth limit in a multimode opto-electromechanical transducer, *Phys. Rev. Appl.* **9**, 034031 (2018).
- [45] C. Gonzalez-Ballester, D. Hümmer, J. Giese, and O. Romero-Isart, Theory of quantum acoustomagnonics and acoustomechanics with a micromagnet, *Phys. Rev. B* **101**, 125404 (2020).
- [46] X. Zhang, C. L. Zou, L. Jiang, and H. X. Tang, Cavity magnomechanics, *Sci. Adv.* **2**, e1501286 (2016).
- [47] C. W. Gardiner and P. Zoller, *Quantum Noise* (Springer, Berlin, 2000).
- [48] J. B. Johnson, Thermal agitation of electricity in conductors, *Phys. Rev.* **32**, 97 (1928).
- [49] H. Nyquist, Thermal agitation of electric charge in conductors, *Phys. Rev.* **32**, 110 (1928).
- [50] E. X. DeJesus and C. Kaufman, Routh-Hurwitz criterion in the examination of eigenvalues of a system of nonlinear ordinary differential equations, *Phys. Rev. A* **35**, 5288 (1987).
- [51] A. Sohail, M. Rana, S. Ikram, T. Munir, T. Hussain, R. Ahmed, and C. S. Yu, Enhancement of mechanical entanglement in hybrid optomechanical system, *Quantum Inf. Process.* **19**, 372 (2020).
- [52] A. Sohail, R. Ahmed, C. S. Yu, and T. Munir, Enhanced entanglement induced by Coulomb interaction in coupled optomechanical systems, *Phys. Scr.* **95**, 035108 (2020).
- [53] J. Eisert, *Entanglement in Quantum Information Theory* (University of Potsdam, Potsdam, 2001).
- [54] G. Vidal and R. F. Werner, Computable measure of entanglement, *Phys. Rev. A* **65**, 032314 (2002).
- [55] M. B. Plenio, Logarithmic negativity: A full entanglement monotone that is not convex, *Phys. Rev. Lett.* **95**, 090503 (2008).
- [56] G. Adesso and F. Illuminati, Entanglement in continuous-variable systems: recent advances and current perspectives, *J. Phys. A* **40**, 7821 (2007).
- [57] S. Zheng, F. Sun, Y. Lai, Q. Gong, and Q. He, Manipulation and enhancement of asymmetric steering via interference effects induced by closed-loop coupling, *Phys. Rev. A* **99**, 022335 (2019).
- [58] I. Kogias, A. R. Lee, S. Ragy, and G. Adesso, Quantification of Gaussian quantum steering, *Phys. Rev. Lett.* **114**, 060403 (2015).
- [59] G. Adesso and F. Illuminati, Continuous variable tangle, monogamy inequality, and entanglement sharing in Gaussian states of continuous variable systems, *New J. Phys.* **8**, 15 (2006).
- [60] V. Coffman, J. Kundu, and W. K. Wootters, Distributed entanglement, *Phys. Rev. A* **61**, 052306 (2000).
- [61] H. J. Cheng, S. J. Zhou, J. X. Peng, A. Kundu, H. X. Li, L. Jin, and X. L. Feng, Tripartite entanglement in a Laguerre–Gaussian rotational-cavity system with an

- yttrium iron garnet sphere, *J. Opt. Soc. Am. B* **38**, 285 (2021).
- [62] A. Sohail, Z. Abbas, R. Ahmed, A. Shahzad, N. Akhtar, and J. X. Peng, Enhanced entanglement and controlling quantum steering in a Laguerre-Gaussian cavity optomechanical system with two rotating mirrors, *Eur. Phys. J. Plus* **138**, 417 (2023).
- [63] V. Händchen, T. Eberle, S. Steinlechner, A. Sambrowski, T. Franz, R. F. Werner, and R. Schnabel, Observation of one-way Einstein–Podolsky–Rosen steering, *Nat. Photonics* **6**, 596 (2012).
- [64] K. Sun, J. S. Xu, X. J. Ye, Y. C. Wu, J. L. Chen, C. F. Li, and G. C. Guo, Experimental demonstration of the Einstein–Podolsky–Rosen steering game based on the all-versus-nothing proof, *Phys. Rev. Lett.* **113**, 140402 (2014).
- [65] Y. Kajiwara, K. Harii, S. Takahashi, J. Ohe, K. Uchida, M. Mizuguchi, H. Umezawa, H. Kawai, K. Ando, K. Takanashi, S. Maekawa, and E. Saitoh, Transmission of electrical signals by spin-wave interconversion in a magnetic insulator, *Nature* **464**, 262 (2010).
- [66] B. Rana and Y. Otani, Towards magnonic devices based on voltage-controlled magnetic anisotropy, *Commun. Phys.* **2**, 90 (2019).
- [67] Y. Wei and B. Wang, Generation of higher-order sidebands based on the magnetostrictive interaction in a hybrid cavity electro–opto–magnomechanical system, *JOSA B* **37**, 218 (2020).
- [68] S. Romyantsev, M. Balinskiy, F. Kargar, A. Khitun, and A. A. Balandin, The discrete noise of magnons, *Appl. Phys. Lett.* **114**, 090601 (2019).
- [69] A. Furusawa, J. L. Sorensen, S. L. Braunstein, C. A. Fuchs, H. J. Kimble, and E. S. Polzik, Unconditional quantum teleportation, *Science* **282**, 706 (1998).
- [70] A. Calabrese, D. Gacemi, M. Jeannin, S. Suffit, A. Vasanelli, C. Sirtori, and Y. Todorov, Coulomb forces in THz electromechanical meta-atoms, *Nanophotonics* **8**, 2269 (2019).
- [71] H. Y. Yuan, Y. Cao, A. Kamra, R. A. Duine, and P. Yan, Quantum magnonics: When magnon spintronics meets quantum information science, *Phys. Rep.* **965**, 1 (2022).
- [72] M. Wang, X. Y. Lü, J. Y. Ma, H. Xiong, L. G. Si, and Y. Wu, Controllable chaos in hybrid electro-optomechanical systems, *Sci. Rep.* **6**, 22705 (2016).
- [73] M. Wallquist, K. Hammerer, P. Rabl, M. Lukin, and P. Zoller, Hybrid quantum devices and quantum engineering, *Phys. Scr.* **2009**, 014001 (2009).